



## Anomalous conductivity due to two-stream instability in bilayer graphene

Vasco Pinhão ,\* Pedro Cosme , and Hugo Terças <sup>†</sup>

GoLP | Instituto de Plasmas e Fusão Nuclear, Instituto Superior Técnico, Universidade de Lisboa, 1049-001 Lisbon, Portugal



(Received 14 April 2023; revised 14 July 2023; accepted 4 August 2023; published 17 August 2023)

We investigate the electron-hole two-stream instability (or Coulomb drag) in bilayer graphene in the hydrodynamic regime, accounting for the effects of temperature, initial drift velocity, magnetic field, and collisions. We put in evidence a purely electrostatic mechanism leading to current relaxation, giving rise to a well-defined dc longitudinal conductivity  $\propto T^{3/2}$ . Due to competition between electrostatic and collisional processes, two distinct transport regimes are identified. An analysis on the Hall conductivity revealed that the two-stream instability effects also correct the most recent results obtained within the linear response theory.

DOI: [10.1103/PhysRevB.108.L081406](https://doi.org/10.1103/PhysRevB.108.L081406)

**Introduction.** The study of graphene samples of extreme purity has led to the realization of an electronic regime that was first proposed theoretically in the 1960s, namely, the hydrodynamic regime [1]. In this regime, electron-electron collisions dominate over scattering with disorder and electronic dynamics can be described with fluid equations. While the hydrodynamics of monolayer graphene has been extensively studied [2–7], the validity of hydrodynamic regimes for electrons in graphene bilayers is fairly recent [8,9]. The hydrodynamic behavior of graphene has been a subject of interest in recent years, particularly the electron-hole Coulomb drag [10,11], which has been shown to play a significant role in the transport properties near the Dirac point—or at charge neutrality (CN) [12,13]. Experimental and theoretical works on Coulomb drag have shown that the drag resistivity is strongly dependent on temperature, doping, magnetic field, and interlayer coupling strength [14–19]. For instance, recent studies have shown that the Coulomb drag between two well separated graphene sheets can give rise to interesting phenomena, such as increasing of drag resistivity of graphene heterostructures at low temperatures [20], anomalous resistivity scaling when the two layers are kept at different temperatures [21], and the emergence of new transport regimes in the presence of a magnetic field [22]. However, the hydrodynamic regime in bilayer graphene structures at CN has not been fully addressed, with few examples reporting on the quadratic scaling of the resistivity with temperature [23,24], especially regarding the late stages (saturation) of the electrostatic instabilities.

In this Letter, we investigate the electron-hole two-stream instability taking place at CN in bilayer graphene, previously studied in systems composed of two well separated layers [10]. We show that, below a critical temperature, in which an electrostatic instability is found to take place, there is a strong suppression of the conductivity due to the electrostatic turbulence generated in the instability process. Conversely, above that critical temperature, the conductivity matches the

one expected from a linear response theory [9]. Our findings may have important consequences in applications with bilayer graphene devices operating at the neutrality point and also pave the stage towards the investigation of electrostatic turbulence in Coulomb drag configurations.

**Two-fluid model.** In light of the quadratic dispersion of the low-lying quasiparticles in AB-stacking bilayer graphene (BLG),  $\epsilon_{e,h}(\mathbf{p}) = \pm |\mathbf{p}|^2/2m_{e,h}$ , of effective mass  $m_{e,h} \equiv m \simeq 0.033m_0$  [25], with  $m_0$  being the bare electron mass, the fluid equations can be obtained from a quantum kinetic model [9] and recast as

$$\begin{aligned} \frac{\partial n_\nu}{\partial t} + \nabla \cdot \mathbf{j}_\nu &= 0, \quad \nu = \{e, h\}, \\ \frac{\partial \mathbf{j}_\nu}{\partial t} + \nabla \cdot \left( \frac{\mathbf{j}_\nu \otimes \mathbf{j}_\nu}{n_\nu} + \frac{\mathbb{P}_\nu}{m} \right) &= \frac{q_\nu}{m} (n_\nu \mathbf{E} + \mathbf{j}_\nu \times \mathbf{B}_0) + n_\nu \frac{\mathbf{F}_\nu^{\text{col}}}{m}. \end{aligned} \quad (1)$$

In our analysis, we neglect the effects of the trigonal warping, which has been shown to be relevant away from the charge neutrality point and for very low temperatures,  $T \lesssim 10$  K [26,27]. Here,  $\mathbf{j}_\nu = n_\nu \mathbf{v}_\nu$  is the current density,  $q_{e,h} = \mp e$  is the electron/hole charge, and  $\mathbb{P}_\nu = P_\nu \mathbb{I}$  is the pressure dyad of the  $\nu$ th species. The electric field  $\mathbf{E} = \mathbf{E}_{\text{sc}} + \mathbf{E}_0$  comprises a self-consistent portion  $\mathbf{E}_{\text{sc}}$  and an externally applied dc field  $\mathbf{E}_0$ ,  $\mathbf{B}_0$  is the transverse magnetic field, and  $\mathbf{F}_\nu^{\text{col}}$  encodes the processes of momentum dissipation. Under weak perturbations, the relaxation time approximation can be applied, leading to

$$\mathbf{F}_\nu^{\text{col}} = \mathbf{F}_{\nu,\nu'} + \mathbf{F}_{\nu,\text{dis}} \approx -\frac{\mathbf{v}_\nu - \mathbf{v}_{\nu'}}{\tau_{\nu,\nu'}} - \frac{\mathbf{v}_\nu}{\tau_{\text{dis},\nu}}. \quad (3)$$

Notice that the intraspecies collision terms are absent because they conserve the total fluid momentum. The collision times can be given as  $\tau_{\nu,\nu'} = \tau_0(n_\nu + n_{\nu'})/n_\nu$ , where  $\tau_0^{-1} \simeq 0.15k_B T/\hbar$  [9]. Motivated by experiments [28], we neglect the contribution due to impurities, resulting in a Matthiessen rule of the form  $\tau_{\text{dis},\nu}^{-1} = \tau_{\text{ph},\nu}^{-1} + \tau_{\text{imp},\nu}^{-1} \simeq \tau_{\text{ph},\nu}^{-1}$ , and electron-phonon collision time can be estimated as  $\tau_{\text{ph}}^{-1} \simeq 0.05k_B T/\hbar$ .

To close Eqs. (1) and (2) with an equation of state, we resort to the local quasiequilibrium hypothesis [4] by assuming

\*vasco.pinhao@tecnico.ulisboa.pt

<sup>†</sup>hugo.tercas@tecnico.ulisboa.pt

the two species to be distributed according to a drifting Fermi-Dirac distribution [29]. In terms of the inverse temperature  $\beta_v = 1/(k_B T_v)$  and the chemical potential  $\mu_v$ , the densities read

$$n_v(\mathbf{x}, t) = \frac{N_f m}{2\pi \beta_v \hbar^2} \ln(1 + e^{\beta_v \mu_v}), \quad (4)$$

where  $N_f = 4$  accounts for spin and valley degeneracy [25]. We then invert the expression in (4) to write the chemical potential as a function of density and plug the result into the pressure to obtain

$$P_v = -\frac{N_f m}{2\pi \beta_v^2 \hbar^2} \text{Li}_2 \left[ 1 - \exp \left( n_v \frac{2\pi \beta_v \hbar^2}{N_f m} \right) \right], \quad (5)$$

with  $\text{Li}_2$  being the polylogarithm function of second order. Below, we shall set  $\beta_e^{-1} = \beta_h^{-1} = k_B T$ .

*Euler-Poisson system.* In the long-wavelength limit  $kd \ll 1$ , with  $\mathbf{k} = (k_x, k_y)$  being the wave vector,  $k = |\mathbf{k}|$ , and  $d \sim 1 \text{ \AA}$  the interlayer spacing, the self-consistent electric field  $\mathbf{E}_{\text{sc}} = -\nabla\phi$  can be written in terms of the electrostatic field  $\phi$ , and its Fourier transform reads

$$\phi(\mathbf{k}) = \frac{e}{2\epsilon k} [n_h(\mathbf{k}) - n_e(\mathbf{k})], \quad (6)$$

where  $\epsilon$  is the dielectric permittivity of the substrate (for the sake of numerical illustration, we set  $\epsilon = \epsilon_0$  in the remainder of the manuscript). Additionally, we introduce the system size  $L$  and the screening length  $\lambda_{\text{scr}} = \pi \epsilon_0 \hbar^2 / [\ln(2)e^2 m] \approx 5.8 \text{ \AA}$ , which sets the typical scale of charge imbalance in the plasma. In our study, we consider conditions in which the system is much larger than the screening length,  $L \gg \lambda_{\text{scr}}$ .

*Two-stream instability.* The two-stream instability is a trademark instability in classical plasma physics, which is excited by placing two particle populations with a relative drift velocity in contact, e.g., a cold electron beam impinging on a steady plasma [31] or two counter-propagating beams. In the present electron-hole plasma, both species have equal mass; the dc electric field  $\mathbf{E}_0$  will drive the electrons and holes in opposite directions with the same drift velocity, thus triggering a hydrodynamical instability. To illustrate this effect in bilayer graphene, we proceed to the direct numerical simulation of the two-fluid mode in Eqs. (1) and (2), together with Eqs. (5) and (6), with the help of TETHYS [32–34]. Our algorithm consists in a finite-volume method with a semi-implicit scheme [35–37], advancing the force terms implicitly and the flux terms explicitly [38,39]. More precisely, the fluxes are estimated with a third-order monotonic upstream-centered scheme for conservation laws (MUSCL) [40], coupled to a min-mod slope limiter [41], and then computing the fluxes at the boundaries using the Harten–Lax–van Leer–Contact (HLLC) flux [40,42]. The time evolution is carried out with a third-order total variation diminishing (TVD) Runge-Kutta method [43]. A signature of this process is the formation of charge bunches in the linear stages of the instability, as depicted in Fig. 1(a). At the late stages, quasineutrality is restored globally and the bunches coalesce, leading to saturation of the instability [see Fig. 1(b)], which we address later on.

To investigate the instability conditions analytically, we perform a linear analysis of the two-fluid model, by considering perturbations of frequency  $\omega$  and momentum  $k$  on top of

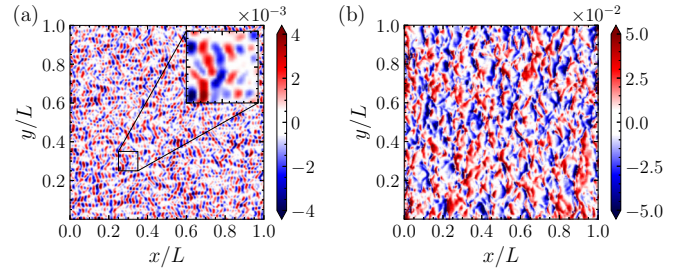


FIG. 1. Two-stream instability in bilayer graphene. (a) Charge imbalance density at the linear phase of the instability ( $t = 0.016L/v_{50}$ ) [30], highlighting the formation of charge bunches in the inset. (b) Charge imbalance density at the nonlinear phase of the instability ( $t = 0.18L/v_{50}$ ). The simulations were performed on a  $256 \times 256$  grid with periodic boundaries for  $v_0/v_{50} = 3.0$  and  $L = 1000 \lambda_{\text{scr}}$ .

an electron-hole fluid counterstreaming with initial velocities  $\mathbf{v}_{e,h} = \pm v_0 \mathbf{e}_x$  and initial charge densities set to their value at charge neutrality, i.e., Eq. (4) evaluated at zero chemical potential. Instability occurs provided the condition

$$\omega^2 = -\sqrt{q_{\text{scr}}^2 v_{\text{th}}^4 k^2 + 4q_{\text{scr}} k_x^2 v_0^2 v_{\text{th}}^2 k + 4k_x^2 v_0^2 [v_{\text{th}}^2 \ln(4) k^2 + \omega_c^2]} + q_{\text{scr}} v_{\text{th}}^2 k + v_{\text{th}}^2 \ln(4) k^2 + k_x^2 v_0^2 + \omega_c^2 < 0, \quad (7)$$

where  $v_{\text{th}} = \sqrt{k_B T/m}$  is the thermal velocity,  $q_{\text{scr}} = \lambda_{\text{scr}}^{-1}$  is the effective screening wave number, and  $\omega_c = eB/m$  is the cyclotron frequency. We observe that the unstable mode has a vanishing real part, thus behaving as a purely growing (stationary) wave of growth rate  $\gamma \equiv \text{Im}(\omega)$ . The threshold condition in  $\gamma = 0$  can be expressed as  $v_0 > v_{\text{min}}(\theta)$ , where

$$v_{\text{min}}(\theta) \equiv \sqrt{\frac{\omega_c^2}{k_x^2} + \frac{v_{\text{th}}^2 \ln(4)}{\cos^2(\theta)}} \quad (8)$$

and  $\theta = \arctan(k_y/k_x)$  is the angle of  $\mathbf{k}$  with respect to the  $x$  axis. The cutoff velocity in Eq. (8) is always finite for finite temperature and tends to the critical velocity  $v_C \equiv \sqrt{v_{\text{th}}^2 \ln(4)} \approx 1.117 v_{\text{th}}$  as  $\theta \rightarrow 0$ , which equals the first-sound

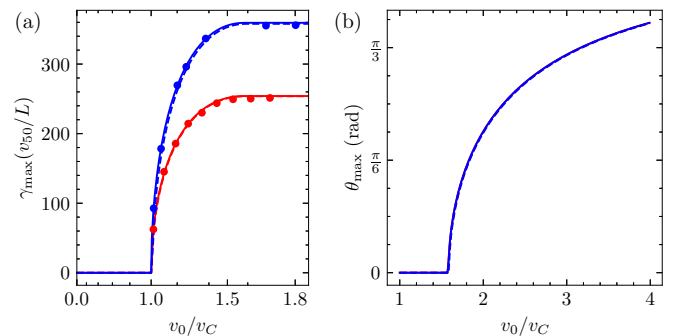


FIG. 2. (a) Maximum growth rate as a function of  $v_0/v_C$  for  $T = 50 \text{ K}$  and  $T = 100 \text{ K}$  (red and blue lines, respectively), and  $B = 0, 2, 5 \text{ T}$  (solid blue and red lines, dashed red line, and dashed blue line, respectively). The numerical estimates (dots) for  $B = 0$  are superimposed. (b) Orientation of the wave vector corresponding to the most unstable mode. The same identification applies (note that the solid lines overlap). For illustration, we have set  $k_{\text{max}} = 64 \times 2\pi/L$ .

velocity of a 2D Fermi gas,  $v_C = \sqrt{(\partial P_v / \partial n_v) / m}$  [44,45]. A qualitative rationale behind this threshold follows like this: for sufficiently slow drifts, the thermal motion dominates, and so the particles tend to move incoherently, preventing the coherent excitation needed for the instability [46].

Another interesting feature of the instability is the most unstable mode  $\mathbf{k}_{\max} = k_{\max}(\cos \theta_{\max}, \sin \theta_{\max})$ , which maximizes the growth rate, such that  $\gamma_{\max} \equiv \gamma(\mathbf{k}_{\max})$ , for a set of external parameters ( $v_0, T, \omega_c$ ). While  $\gamma_{\max}$  is a growing function of  $k$ ,  $k_{\max}$  should not be larger than the thermal wave number and the inverse electron mean-free path, where the hydrodynamic description fails. In practice, we should

$$v_{\text{peak}} \equiv \frac{\sqrt{\{k v_{\text{th}}^2 [q_{\text{scr}} + k \ln(16)] + 2\omega_c^2\} \{k v_{\text{th}}^2 [3q_{\text{scr}} + k \ln(16)] + 2\omega_c^2\}}}{2k \sqrt{k v_{\text{th}}^2 [q_{\text{scr}} + k \ln(4)] + \omega_c^2}}. \quad (9)$$

Hence the maximum growth rate  $\gamma_{\max}$  is obtained by evaluating  $\gamma$  at the peak velocity. In the long wavelength limit  $k \ll q_{\text{scr}}$ , it simply reads  $\gamma_{\max} \simeq v_{\text{th}} \sqrt{k q_{\text{scr}}} / 2$ . For modes close to the instability threshold, the effect of collisions will eventually become noticeable but, for most temperatures, as the initial velocity is increased, there will still be available modes that are just slightly affected by collisions. This stops being the case when the maximum growth rate at a given temperature is of the order of the collision frequency, which occurs when

$$T \geq T_{\text{col}} \equiv 16 \frac{\hbar^2 q_{\text{scr}}}{m k_B} k. \quad (10)$$

We observe that only for very small wave numbers do collisions start contributing significantly to the damping of the growing waves near room temperatures.

A final comment regarding the effect of magnetic field. We notice that the validity of a semiclassical description, i.e., away from Landau levels [9], bounds the admissible values of the magnetic field: for temperatures ranging as  $T = 50\text{--}100$  K, it should not exceed 2–5 T. As shown in Fig. 2(a), the magnetic field plays no significant role in the instability growth rate. Like collisions, only for very large wavelengths should we start observing significant effects. In any case, away from the weak field limit, the hydrodynamic model becomes again incomplete: even away from the Landau level (quantum) limit, kinetic effects should take place, giving rise to a hierarchy of modes called Bernstein modes [22,47].

In order to corroborate our analytical estimates, we extract  $\gamma$  numerically by fitting the most unstable Fourier mode of the electric field,  $|E_{\mathbf{k}_{\max}}|$ , in the linear stages (see Fig. 3). We employ periodic boundary conditions for all hydrodynamic variables and initially add a small density perturbation whose amplitude is  $\simeq 5\%$  of its value at CN to simulate the naturally occurring random density fluctuations. The comparison depicted in Fig. 2 shows an excellent agreement with the simulations.

*Nonlinear transport properties.* In the simulations performed in this section, both species start at rest and accelerate under the influence of an external electric field  $E_0$  of varying magnitude, with the remaining initial conditions left un-

consider  $k \ll q_{\text{scr}}$ . Otherwise, in Fig. 2(b) we observe that the most unstable mode is aligned with the flow at the threshold, but as  $v_0$  increases, it rotates and tends asymptotically to  $\theta = \pi/2$ . Interestingly, the most unstable directions for different temperatures collapse onto each other when plotted as a function of  $v_0/v_C$ , so the angle is a universal function of this quantity. Coincidentally, the rotation is also accompanied by a stabilization of the maximum growth rate, as illustrated in Fig. 2(a), meaning that  $\gamma_{\max}$  stops depending on  $v_0$  when the most unstable wave vector develops a transverse component. Then, we set  $k_y = 0$  in Eq. (7) and minimize the expression with respect to  $v_0$  to find the peak velocity

changed. Within the linear theory developed in [9], the dc longitudinal conductivity  $\sigma_{xx} = j_x/E_0^x$  was found to be independent of temperature in the sole presence of Coulomb drag and phonon collisions. At charge neutrality, the dc conductivity reads

$$\sigma_{xx}^{\text{CN}} = \frac{2 \ln(32) N_f e^2}{\pi 2\hbar} \simeq 2.206 \frac{N_f e^2}{2\hbar}. \quad (11)$$

Throughout this section, the current we refer to is the total electric current density  $\mathbf{j} = e(n_h \mathbf{v}_h - n_e \mathbf{v}_e)$ . In the absence of a magnetic field and at CN, the linear theory predicts that a steady state is reached when the fluids reach the steady-state velocity  $v_h = -v_e \equiv v_\infty$ , where  $v_\infty = 5\hbar E_0 / m k_B T$ . As such, the effects of the two-stream instability are expected to take place if  $v_\infty > v_{\text{min}}$ , which translates into the condition

$$T \leq T_C \equiv \left( \frac{25}{\ln(4)} \frac{e^2 \hbar^2}{m k_B^3} E_0^2 \right)^{\frac{1}{3}}. \quad (12)$$

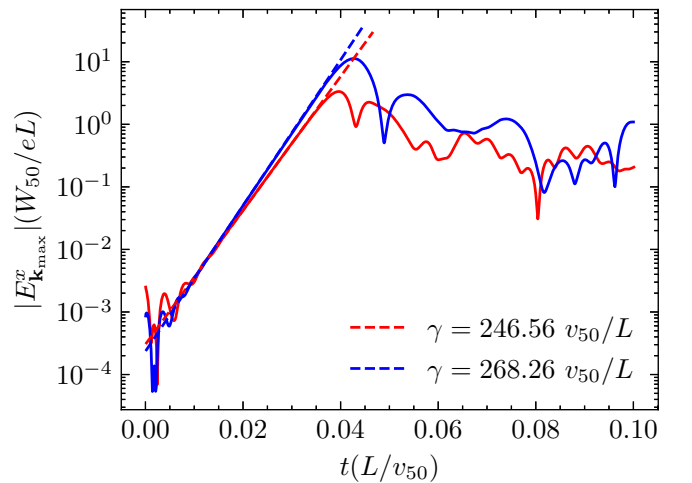


FIG. 3. Time evolution of the most unstable Fourier coefficient of the longitudinal electric field for  $v_0/v_{50} = 2.0$  and  $B = 0$ , for  $T = 50$  K (red line) and  $T = 100$  K (blue line). The dashed lines are the exponential fit in the linear regime. The simulation was performed on a  $1024 \times 1024$  grid with periodic boundaries.

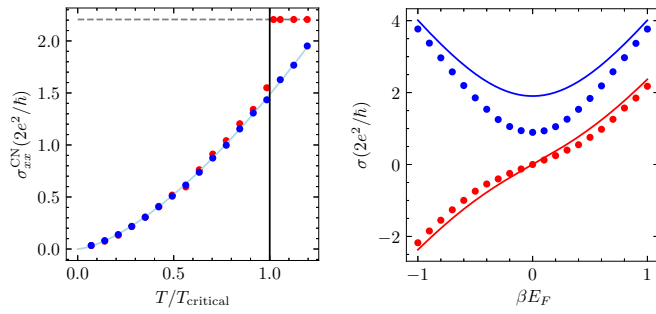


FIG. 4. Left: conductivity at charge neutrality as a function of temperature in the collisionless (blue dots) and collisional (red dots) limits. The solid line is the best-fitted ansatz for the collisionless case and the dashed line represents the conductivity in Eq. (11). Right: transverse (red) and longitudinal (blue) conductivities in the linear (solid line) and nonlinear regimes (dots) as a function of  $\beta E_F$  for  $T = 50$  K and  $B = 0.05$  T. In both plots, we set  $E_0 = 74.4$  kV/m.

Alternatively, under experimental conditions where the temperature is kept constant, it is possible to define a critical applied field triggering instability as

$$E_0 \geq E_{0,C} \equiv \frac{\sqrt{\ln(4)}}{5} \left( \frac{k_B^{3/2} m^{1/2}}{e\hbar} \right) T^{3/2}. \quad (13)$$

The plasma modes amplified by the two-stream instability absorb energy from the translational degrees of freedom. Deep into the nonlinear stages, i.e., after the formation of the plateau in Fig. 3, an electrostatic turbulent spectrum builds up as a consequence of the nonlinear wave interactions, leading to the termination of the instability [48]. In this saturation regime, the power supplied by the external electric field in the form of Joule heating  $\mathbf{j} \cdot \mathbf{E}_0$  is appropriately redistributed among the plasma oscillations and the kinetic and thermal energy, producing an oscillating quasisteady state. In other words, the two-stream instability suppresses the conductivity of the electron-hole plasma.

Motivated by the performed simulations, we propose a phenomenological ansatz for the saturation current of the form

$$j_x^{\text{sat}} = \mathcal{A} j_x^{\text{min}} = 2\mathcal{A} e n_0 \sqrt{\ln(4) \frac{k_B T}{m}} \propto T^{3/2}, \quad (14)$$

where  $\mathcal{A}$  is a numerical factor,  $j_x^{\text{min}} \approx 2en_0v_C$  is the threshold current, and  $n_0 \sim T$  is the density, as given by Eq. (4). This guess is justified because the drift velocity saturates near  $v_C$ ; hence the temperature dependence of the two currents should not vary appreciably and the fact that, near the threshold for instability, the growth rate of the unstable modes is similar for each temperature, thus so should be the percentage of dissipated current. The fit shown in Fig. 4(a) provides  $\mathcal{A}(L =$

$100\lambda_{\text{scr}}) = 0.67$ , meaning that about 33% of the current at the onset of instability is dissipated. For better screening, there is a larger energy transfer to the unstable waves, which establishes a lower saturation current: e.g.,  $\mathcal{A}(L = 1000\lambda_{\text{scr}}) = 0.44$ . In addition, stronger electric fields promote overshoots of the saturated velocity past  $v_C$ , enabling further current dissipation as more energetic modes are excited: for instance, the saturation current close to the critical electric field for  $T = 50$  K is  $j_x^{\text{sat}} \simeq 1.81n_{50}v_{50}$  (in simulation units), whereas for  $E_0 = W_{50}/(eL) \approx 74.4$  kV/m it is  $\sim 1.65n_{50}v_{50}$ , exhibiting an obvious decline.

When collisions are introduced, two distinct regimes can be identified in Fig. 4(a). Before the critical temperature,  $\sigma_{xx}$  follows the power law in Eq. (14). After that value, we enter the linear regime, where the conductivity becomes constant with temperature, taking on the value predicted in Eq. (11). Comparing the Hall conductivity Fig. 4(b) with the one obtained within the linear regime, we witness that there is a small suppression of the conductivity, but the overall shape remains the same. The same occurs for the longitudinal conductivity, but the suppression is more noticeable, particularly for small charge imbalances. Close to the threshold for instability, the transverse component of the unstable modes is much smaller than the longitudinal one, resulting in less dissipation of current due to the two-stream mechanism along the  $y$  direction.

*Conclusions.* A hydrodynamic theory of the two-stream instability in bilayer graphene was put forward. We have demonstrated the existence of a threshold drift speed, close to the thermal speed, controlling the onset of the instability of the electron-hole plasma at charge neutrality. At the nonlinear, late times, stages of the instability, the electrostatic field produced is responsible to the suppression of the conductivity. We have also observed that a transverse magnetic field and collisions quench the instability growth rate but, for typical parameters, their role only becomes apparent for very long wavelength modes. The theoretical predictions were confirmed numerically, validating the used scheme.

In the isothermal regime, two distinct regimes dominated either by electrostatic or collisional processes have been identified. In the first, the conductivity scales as  $\propto T^{3/2}$  at charge neutrality, contrasting with the temperature-independent value predicted by the linear theory. Away from charge neutrality, both  $\sigma_{xx}$  and  $\sigma_{xy}$  are suppressed relative to the linear case, although the first is more severely suppressed. Our findings open the venue for the implications of nonlinear response in the determination of other relevant physical quantities.

*Acknowledgments.* H.T. acknowledges Fundação para a Ciência e a Tecnologia (FCT-Portugal) through Contract No. CEECIND/00401/2018 and through Project No. PTDC/FIS-OUT/3882/2020. P.C. acknowledges the funding provided by Fundação para a Ciência e a Tecnologia (FCT-Portugal) through Grant No. PD/BD/150415/2019.

- [1] R. N. Gurzhi, *Sov. Phys. Usp.* **11**, 255 (1968).  
 [2] D. Svintsov, V. Vyurkov, S. Yurchenko, T. Otsuji, and V. Ryzhii, *J. Appl. Phys.* **111**, 083715 (2012).  
 [3] D. Svintsov, V. Vyurkov, V. Ryzhii, and T. Otsuji, *Phys. Rev. B* **88**, 245444 (2013).

- [4] A. Lucas and K. C. Fong, *J. Phys.: Condens. Matter* **30**, 053001 (2018).  
 [5] J. A. Sulpizio, L. Ella, A. Rozen, J. Birkbeck, D. J. Perello, D. Dutta, M. Ben-Shalom, T. Taniguchi, K. Watanabe, T. Holder, R. Queiroz, A. Principi, A. Stern, T. Scaffidi,

- A. K. Geim, and S. Ilani, *Nature (London)* **576**, 75 (2019).
- [6] B. N. Narozhny and I. V. Gornyi, *Front. Phys.* **9**, 640649 (2021).
- [7] J. L. Figueiredo, J. P. S. Bizarro, and H. Terças, *New J. Phys.* **24**, 023026 (2022).
- [8] D. Y. H. Ho, I. Yudhistira, N. Chakraborty, and S. Adam, *Phys. Rev. B* **97**, 121404(R) (2018).
- [9] D. X. Nguyen, G. Wagner, and S. H. Simon, *Phys. Rev. B* **101**, 035117 (2020).
- [10] B. N. Narozhny and A. Levchenko, *Rev. Mod. Phys.* **88**, 025003 (2016).
- [11] D. Y. H. Ho, I. Yudhistira, B. Y.-K. Hu, and S. Adam, *Commun. Phys.* **1**, 41 (2018).
- [12] E. H. Hwang, R. Sensarma, and S. Das Sarma, *Phys. Rev. B* **84**, 245441 (2011).
- [13] R. V. Gorbachev, A. K. Geim, M. I. Katsnelson, K. S. Novoselov, T. Tudorovskiy, I. V. Grigorieva, A. H. MacDonald, S. V. Morozov, K. Watanabe, T. Taniguchi, and L. A. Ponomarenko, *Nat. Phys.* **8**, 896 (2012).
- [14] W.-K. Tse, B. Y.-K. Hu, and S. Das Sarma, *Phys. Rev. B* **76**, 081401(R) (2007).
- [15] S. Kim and E. Tutuc, *Solid State Commun.* **152**, 1283 (2012).
- [16] S. M. Badalyan and F. M. Peeters, *Phys. Rev. B* **86**, 121405(R) (2012).
- [17] M. Schütt, P. M. Ostrovsky, M. Titov, I. V. Gornyi, B. N. Narozhny, and A. D. Mirlin, *Phys. Rev. Lett.* **110**, 026601 (2013).
- [18] D. A. Bandurin, I. Torre, R. K. Kumar, M. B. Shalom, A. Tomadin, A. Principi, G. H. Auton, E. Khestanova, K. S. Novoselov, I. V. Grigorieva, L. A. Ponomarenko, A. K. Geim, and M. Polini, *Science* **351**, 1055 (2016).
- [19] P. Simonet, S. Hennel, H. Overweg, R. Steinacher, M. Eich, R. Pisoni, Y. Lee, P. Märki, T. Ihn, K. Ensslin, M. Beck, and J. Faist, *New J. Phys.* **19**, 103042 (2017).
- [20] A. Gamucci, D. Spirito, M. Carrega, B. Karmakar, A. Lombardo, M. Bruna, L. N. Pfeiffer, K. W. West, A. C. Ferrari, M. Polini, and V. Pellegrini, *Nat. Commun.* **5**, 5824 (2014).
- [21] F. Escudero, F. Arreyes, and J. S. Ardenghi, *Phys. Rev. B* **106**, 245414 (2022).
- [22] X. Liu, L. Wang, K. C. Fong, Y. Gao, P. Maher, K. Watanabe, T. Taniguchi, J. Hone, C. Dean, and P. Kim, *Phys. Rev. Lett.* **119**, 056802 (2017).
- [23] J. Lux and L. Fritz, *Phys. Rev. B* **87**, 075423 (2013).
- [24] J. I. A. Li, T. Taniguchi, K. Watanabe, J. Hone, A. Levchenko, and C. R. Dean, *Phys. Rev. Lett.* **117**, 046802 (2016).
- [25] E. McCann and M. Koshino, *Rep. Prog. Phys.* **76**, 056503 (2013).
- [26] E. McCann and V. I. Fal'ko, *Phys. Rev. Lett.* **96**, 086805 (2006).
- [27] G. Wagner, D. X. Nguyen, and S. H. Simon, *Phys. Rev. Lett.* **124**, 026601 (2020).
- [28] Y. Nam, D.-K. Ki, D. Soler-Delgado, and A. F. Morpurgo, *Nat. Phys.* **13**, 1207 (2017).
- [29] J. Crabb, X. Cantos-Roman, J. M. Jornet, and G. R. Aizin, *Phys. Rev. B* **104**, 155440 (2021).
- [30] In virtue of the range of temperatures reported in [9], from which the experimentally motivated scattering time estimates were extracted, we chose the typical temperature to be  $T_{50} = 50$  K. Then, the typical velocity, density, and energy scales can be defined in a consistent manner:  $v_{50} \equiv \sqrt{k_B T_{50}/m}$ ,  $n_{50} \equiv N_f m k_B T_{50} / (2\pi \hbar^2) \ln 2$ , and  $W_{50} \equiv k_B T_{50}$ , respectively.
- [31] L. E. Thode and R. N. Sudan, *Phys. Rev. Lett.* **30**, 732 (1973).
- [32] P. Cosme and H. Terças, *ACS Photon.* **7**, 1375 (2020).
- [33] P. Cosme and H. Terças, *Appl. Phys. Lett.* **118**, 131109 (2021).
- [34] P. Cosme, J. S. Santos, J. P. Bizarro, and I. Figueiredo, *Comput. Phys. Commun.* **282**, 108550 (2023).
- [35] J. Ferziger and M. Peric, *Computational Methods for Fluid Dynamics* (Springer, Berlin, 2012).
- [36] R. LeVeque, *Finite Volume Methods for Hyperbolic Problems*, Cambridge Texts in Applied Mathematics (Cambridge University Press, Cambridge, UK, 2002).
- [37] C. Hirsch, *Numerical Computation of Internal and External Flows: The Fundamentals of Computational Fluid Dynamics* (Elsevier Science, Amsterdam, 2007).
- [38] P. Degond, H. Liu, D. Savelief, and M.-H. Vignal, *J. Sci. Comput.* **51**, 59 (2012).
- [39] P. Crispel, P. Degond, and M.-H. Vignal, *J. Comput. Phys.* **223**, 208 (2007).
- [40] E. Toro, *Riemann Solvers and Numerical Methods for Fluid Dynamics: A Practical Introduction* (Springer, Berlin, 2009).
- [41] G. Li, D. Bhatia, and J. Wang, *J. Braz. Soc. Mech. Sci. Eng.* **42**, 290 (2020).
- [42] N. Fleischmann, S. Adami, and N. A. Adams, *J. Comput. Phys.* **423**, 109762 (2020).
- [43] S. Gottlieb and C.-W. Shu, *Math. Comput.* **67**, 73 (1998).
- [44] M. Bohlen, L. Sobirey, N. Luick, H. Biss, T. Enss, T. Lompe, and H. Moritz, *Phys. Rev. Lett.* **124**, 240403 (2020).
- [45] A. Tonomi, A. Cappellaro, G. Bighin, and L. Salasnich, *Phys. Rev. A* **103**, L061303 (2021).
- [46] B. Y.-K. Hu and J. W. Wilkins, *Phys. Rev. B* **43**, 14009 (1991).
- [47] R. Roldán, M. O. Goerbig, and J.-N. Fuchs, *Phys. Rev. B* **83**, 205406 (2011).
- [48] D. Pines and J. R. Schrieffer, *Phys. Rev.* **124**, 1387 (1961).